Available online at www.elixirpublishers.com (Elixir International Journal)

Electrical Engineering

Elixir Elec. Engg 156 (2021)55538-55542

ISSN: 2229-712X

Voltage Stability Analysis of Mini-Grid Connected with Wind Farms during Fault

Nweke U.C., Aneke J.I. and Nwoye A.N.

Department of Electrical Engineering, Nnamdi Azikiwe University, Awka, Nigeria.

ARTICLE INFO

Article history:

Received: 7 April 2021;

Received in revised form:

8 July 2021;

Accepted: 19 July 2021;

Keywords

Fault,
Wind Farm,
Voltage Stability,
Pulse Width Modulation
(PWM) Converter,
Reactive Power.

ABSTRACT

This paper presents the solution to the problem of grid voltage instability during occurrence of fault, on a system connected with wind turbine - driven doubly-fed induction generator (DFIG) which supplies alternating current (AC) power to the utility grid. Here, two pulse width modulated voltage source converters are connected back to back between the rotor terminals and utility grid via common direct current (DC) link. The grid side converter controls the power flow between the DC bus and the AC side. It allows the system to be operated in sub-synchronous and super synchronous mode of operation. The rotor excitation is provided by the machine side converter. The model makes use of d-q rotor reference frame using dynamic vector approach for machine model. The controller was implemented by the orientation of the generator stator flux vector along a synchronous reference axis. In this way, constant voltage and frequency was obtained and the generator would supply the active and reactive power demanded for the voltage correction by the load, while the wind turbine will be responsible for achieving power balance in the system. The system is modelled and simulated in the Matlab Simulink environment in such a way that it can be suited for modelling of all types of induction generator configurations. The results of the simulations show that DFIG wind turbines improved the voltage stability of the system through its ability to control reactive power and decouple control of active and reactive power by independently controlling the rotor excitation current especially during fault.

1. Introduction

One of the renewable energy sources, the wind turbines, have been used widely in recent years. The motives behind this common use of wind turbines is not unconnected to their low cost and environment friendly nature. However, when wind turbines are used to produce large power, some problems arise in connecting it to power systems. One of the reasons for this is that sometimes, the changes in load demand make the system unstable. This instability in the power system brings about the voltage and reactive power problems (Shukla, Tripathi, 2014). In Power systems, voltage and reactive power control problems are important for continuous case stability. These problems have been solved through the use of DFIG and power electronic converters.

In the case of smaller installations connected to weak electric grids such as medium voltage distribution networks, power quality problems may become a serious concern because of the proximity of the generators to the loads. The existence of voltage dips is one of the main disturbances related to power quality in distribution networks. In developed countries, it is known that from 75% up to 95% of the industrial sector claims to the electric distribution companies are related to problems originated from this disturbance type (Touaiti, Azza, Jemli, 2015; Abdoune, Aouzellag, Ghedamsi 2016)). These problems arise from the fact that many electrical loads are not stable during a voltage dip. The main idea behind this work is to conduct a voltage stability analysis using an iterative power system simulation package, to evaluate the impact of strategically placed wind generators on distribution systems with respect to the critical voltage variations and collapse margins. This work concludes with the discussion of wind generators excellent options for voltage stability.

2.0 Wind Turbine Model Equations

The wind power can be expressed as a function of wind speed

$$P_W = 0.5\rho C_\rho(\lambda,\theta)A_R V_W^3 \quad (1)$$

Where:

ρ is the air density (Kg/m^2), A_R is the area swept by the rotor (m^2), V_W is the upstream wind speed, C_ρ is the performance coefficient with respect to the speed ratio λ and the pitch angle θ

Where λ_i can be approximated by a function of the tip speed ratio λ, which is given by

$$\frac{1}{\lambda_i} = \frac{1}{\lambda} + 0.002$$

The mechanical torque is given by:

$$T_{mech} = P_m/\omega_W \quad (2)$$

3.0 Model Equations of Doubly-Fed Induction Generator (DFIG)

The basic equations of the doubly-fed induction machine can be established by considering the equivalent circuit of a single stator phase and a single rotor phase, and the mutual coupling the stator and the rotor phases. The voltage vector

E-mail address:stevewart2@gmail.com; anekejude@gmail.com, na.nwoye@unizik.edu.ng

consisting of the voltages drops across the resistances of these phases, and the rate of change of the fluxes linking the stator and rotor phases. The fluxes in turn are related to the current vector via a matrix of inductances, which are not constant but periodic functions of time with the period equal to the rotor's electrical speed $\omega_e = P\omega_m$, which is the product of the number of pole pairs P and the rotor's mechanical speed ω_m. When all of the stator and rotor quantities are transformed to a stationary frame (the d-q frame), using Park transformation, in terms of the stator's and rotor's voltage-pulsation frequencies ω_s and ω_r, respectively, the basic equations can be reduced to a set of four with constant coefficients. Moreover, $\omega_e = \omega_s - \omega_r$ and can be found by measuring ω_s and ω_e, and the slip frequency (the ratio $s = \omega_r/\omega_s$ is the slip) (Ataji, Miura, Ise, Tanaka 2016). Thus, the phase angles relating the direction of the d-q frame and the phase angles of the first of the three stator phases A, B and C, $\theta_r = \theta_s - \theta_e$ and the first of the three rotor phases a, b, and c, θ_r satisfy the relation $\theta_r = \theta_s - \theta_e$, where θ_e is the rotor's electrical angle. The four equations of the DFIG with constant coefficient in the d-q frame are:

$$\left.\begin{aligned} V_{ds} &= R_s i_{ds} + \frac{d\emptyset_{ds}}{dt} - \omega_s \emptyset_{qs} \\ V_{qs} &= R_s i_{qs} + \frac{d\emptyset_{qs}}{dt} - \omega_s \emptyset_{ds} \end{aligned}\right\}, \quad (3)$$

$$\left.\begin{aligned} V_{dr} &= R_r i_{dr} + \frac{d\emptyset_{dr}}{dt} - \omega_r \emptyset_{qr} \\ V_{qr} &= R_r i_{qr} + \frac{d\emptyset_{qr}}{dt} - \omega_r \emptyset_{dr} \end{aligned}\right\} \quad (4)$$

The stator fluxes are related to the stator and rotor currents in the $d-q$ frame as:

$$\left.\begin{aligned} \emptyset_{ds} &= L_s i_{ds} + L_m i_{dr} \\ \emptyset_{qs} &= L_s i_{qs} + L_m i_{qr} \end{aligned}\right\} \quad (5)$$

The rotor fluxes are related to the stator and rotor currents in the $d-q$ frame as:

$$\left.\begin{aligned} \emptyset_{dr} &= L_r i_{dr} + L_m i_{ds} \\ \emptyset_{qr} &= L_q i_{qr} + L_m i_{qs} \end{aligned}\right\} \quad (6)$$

Where, R_s, R_r, L_s , and L_r are the resistances and self-inductances of the stator and rotor windings, and L_m is the mutual inductance between a stator and a rotor phase when they are fully aligned with each other.

The vector control strategy applied to the DFIG consists on making the stator flux in quadrature with the $q-axis$ of the Park reference frame, therefore,

$$\emptyset_s = \emptyset_{ds} \quad \text{and} \quad \emptyset_{ds} = 0 \quad (7)$$

Equations (3) and (4) can be simplified as:

$$\frac{d\emptyset_{ds}}{dt} = -R_s i_{ds} + V_{ds} \quad (8)$$

$$V_{qs} = R_s i_{qs} + \omega_s \emptyset_{ds} \quad (9)$$

$$\frac{d\emptyset_{dr}}{dt} = -R_r i_{dr} + \omega_r \emptyset_{qr} + V_{dr} \quad (10)$$

$$\frac{d\emptyset_{qr}}{dt} = -R_r i_{qr} - \omega_r \emptyset_{dr} + V_{qr} \quad (11)$$

From (5)

$$i_{qs} = -L_m/L_s\, i_{qr} \quad (12)$$

And $$i_{ds} = (\emptyset_{ds} - L_m i_{dr})/L_s \quad (13)$$

By substituting (12) and (13) in (6), we obtain

$$\emptyset_{dr} = (L_r - L_m^2)i_{dr} + L_m/L_s \emptyset_{ds} \quad (14)$$

$$\emptyset_{qr} = L_r\left(1 - L_m^2/(L_s L_r)\right)i_{qr} \quad (15)$$

By introducing the leakage coefficient with:

$$\sigma = 1 - L_m^2/(L_s L_r) \quad (16)$$

then:

$$\emptyset_{dr} = L_r \sigma i_{dr} + L_m/L_s \emptyset_{ds} \quad (17)$$

$$\emptyset_{qr} = L_r \sigma i_{qr} \quad (18)$$

Substituting (17) and (18) in (10) and (11), yield:

$$V_{dr} = R_r i_{dr} + \frac{L_r \sigma i_{dr}}{dt} + \frac{\frac{L_m}{L_s} d\emptyset_{ds}}{dt} - \omega_r L_r \sigma i_{qr} \quad (19)$$

$$V_{qr} = R_r i_{qr} + \frac{L_r \sigma i_{qr}}{dt} + \omega_r L_r \sigma i_{qr} + \frac{L_m}{L_s}\omega_r \emptyset_{ds} \quad (20)$$

Assuming that the stator flux is stationary in the $d-q$ frame (the d-axis is aligned with the stator-flux-linkage vector $\emptyset_s$) and neglecting the stator's resistive voltage drop, so:

$$\emptyset_{ds} = \emptyset_s \ and \ \emptyset_{qs} = 0 \quad (21)$$

Also, $$V_{qs} = 0 \ and \ V_{qs} = V_s \quad (22)$$

From (3)

$V_{qs} = V_s = R_s i_{qs} + \omega_s \emptyset_s$ from which

$$\emptyset_s = (V_s - R_s i_{qs})/\omega_s \quad (23)$$

From (5)

$$\emptyset_{ds} = \emptyset_s = L_s i_{ds} + L_m i_{qr} = (V_s - R_s i_{qs})/\omega_s = L_m i_{ms}$$

Where i_{ms} is defined as

$$i_{ms} = (V_s - R_s i_{qs})/\omega_s L_m = \frac{V_s}{\omega_s L_m} - \left(R_s\left(-\frac{L_m}{L_s i_{qr}}\right)/(\omega_s L_m)\right) \quad (24)$$

Then, the rotor voltage equations given by (19) and (20) are expressed as:

$$V_{dr} = R_r i_{dr} + \frac{L_r \sigma i_{dr}}{dt} + \frac{\frac{L_m}{L_s} d\emptyset_{ds}}{dt} - s\omega_s L_r \sigma i_{qr} \quad (25)$$

$$V_{qr} = \left(R_r + \frac{sL_m^2}{L_s^2 R_s}\right) i_{qr} + L_r \sigma \frac{di_{qr}}{dt} + s\omega_s L_r \sigma i_{dr} + sL_m/L_s V_s \quad (26)$$

Furthermore, the active and reactive components of the power at stator terminals are given by:

$$P_s = V_{ds} i_{ds} + V_{qs} i_{qs} \quad (27a)$$

$$Q_s = V_{qs} i_{qs} - V_{ds} i_{qs} \quad (27b)$$

The active and reactive components of the power at rotor terminals are given by:

$$P_r = V_{dr} i_{dr} + V_{qr} i_{qr} \quad (28a)$$

$$Q_r = V_{qr} i_{qr} - V_{dr} i_{qr} \quad (28b)$$

The electromagnetic reaction torque may be expressed as:

$$T_{el} = \emptyset_{ds} i_{qs} - V_{qs} i_{ds} \quad (29)$$

From (21), (22), (23), and (24):

$$T_{el} = -L_m^2/L_s\left(\frac{V_s}{\omega_s L_m} + \frac{R_s}{\omega_s L_s} i_{qr}\right) i_{qr} \quad (30)$$

And the active power at the stator terminal:

$$P_s = V_s i_{qs} = L_m/L_s V_s i_{qr} \quad (31)$$

The reactive power at the stator terminals:

$$Q_s = V_s i_{ds} = \omega_s L_m^2/L_s\left(\frac{V_s}{\omega_s L_m} + \frac{R_s}{\omega_s L_m} i_{qr}\right)\left(\frac{V_s}{\omega_s L_m} + \frac{R_s}{\omega_s L_m} i_{qr} - i_{dr}\right) \quad (32)$$

If the stator resistance R_s is neglected, then (31) can be expressed as

$$Q_s = \frac{L_m}{L_s V_s i_{dr}} + V_s^2/(\omega_s L_s) \quad (33)$$

4.0 Wind Energy Conversion using DFIG

With the increased penetration level of wind power in the power system, wind turbines have to contribute not only to active power generation but also to the reactive power. The main advantages of DFIG wind turbine is its ability to control reactive power and decouple control of active and reactive power by independently controlling the rotor excitation current. The DFIG can produce or absorb any amount of reactive power to or from the grid within its capacity, to regulate the terminal voltage (Erlich, Feltes, Shewarega 2014). To assist its further integration into the modern power system, it is therefore important to assess its dynamical

behavior, steady state performance, and impacts on the interconnected power network with regard to its reactive power capability and voltage control. The optimum speed of the generator should be selected based on annual wind speed distribution and the size of the power converter.

It is not always possible to operate wind turbine in maximum power point tracking mode and constant pitch control only. For maintaining regulated frequency and voltage in the power system, the generated power should be equal to the demanded power, when the load decreases, the power output from the turbine should reduce to match the load. When the speed is less than the rated speed, the pith angle is always kept at zero and the speed ratio λ is varied and corresponding performance coefficient Cp is calculated to obtain demanded power output from the wind turbine.

The case described in this section illustrates application of SimPower System software to study the steady-state and dynamic performance of 9MW wind farm connected to a distribution system. The wind farm consists of six 1.5MW wind turbines connected to a 11kV distribution system exporting power to a 33kV grid through a 30km 25kV feeder. A 23kV,2MVA plant consisting of a motor load (1.68MW induction motor at 0.93 PF) and of a 200kW resistive load is connected on the same feeder at bus B25. A 500kW load is also connected on the 0.575kV bus of the windfarm. The Simulink model of the DFIG wind farm is illustrated in Figure 3.

5.0 Wind Turbine Modeling

Wind turbines convert the kinetic energy present in the wind into mechanical energy by means of torque production. Since the energy contained by the wind is in the form of kinetic energy, its magnitude depends on the air density and the wind velocity. The wind power developed by the turbine is given by the (34):

$$P = \frac{1}{2} C_p \rho A V^3 \quad (34)$$

Where;

C_p is the Power Co-efficient,

ρ is the air density in kg/m^3,

A is the area of the turbine blades in m^2 and

V is the wind velocity in m/sec.

The power coefficient C_p gives the fraction of the kinetic energy that is converted into mechanical energy by the wind turbine. It is a function of the tip speed ratio λ and depends on the blade pitch angle for pitch-controlled turbines. The tip speed ratio may be defined as the ratio of turbine blade linear speed and the wind speed

$$\lambda = \frac{R\omega}{V} \quad (35)$$

Substituting (35) in (34), we have:

$$P = \frac{1}{2} C_p(\lambda) \rho A \left(\frac{R}{\lambda}\right)^3 \omega^3 \quad (36)$$

The output torque of the wind turbine $T_{turbine}$ is calculated by the following.

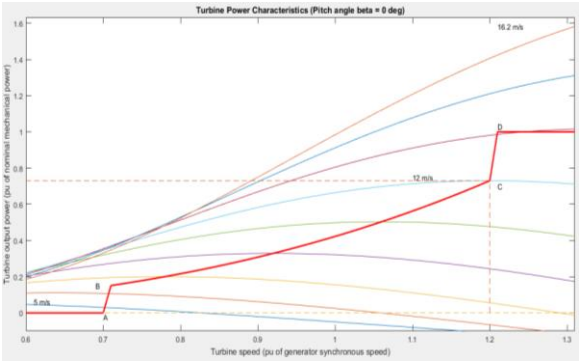

Figure 1. MATLAB Simulink model for wind turbine.

$$T_{turbine} = \frac{1}{2} \rho A C_p V/\lambda \quad (37)$$

Where R is the radius of the wind turbine rotor (m). There is a value of the tip speed ratio at which the power coefficient is maximum. Variable speed turbines can be made to capture this maximum energy in the wind by operating them at a blade speed that gives the optimum tip speed ratio. This may be done by changing the speed of the turbine in proportion to the change in wind speed. Figure 1 shows how variable speed operation will allow a wind turbine to capture more energy from the wind. As one can see, the maximum power follows a cubic relationship. For variable speed generation, an induction generator is considered attractive due to its flexible rotor speed characteristic in contrast to the constant speed characteristic of synchronous generator.

6.0 PWM Voltage Source Inverter Model

The DC power available at the rectifier output is filtered and converted to AC power using a PWM inverter employing double edge sinusoidal modulation (Figure 2). The output consists of a sinusoidally modulated train of carrier opuses, both edges of which are modulated such that the average voltage difference between any two of the output three phases varies sinusoidally. Each edge of the carrier wave is modulated by a variable angle δx and can be mathematically expressed by

$$\delta x = MI \sin(\alpha x)\, \delta_{max} \quad (x = 1, 2, 3 \ldots 2r + 1) \quad (38)$$

Where;

MI is the modulation index and ranges from 0 to 1.

subscript x denotes the edge being considered,

r is the ratio of the carrier to fundamental frequency at the inverter output,

αx is the angular displacement of the unmodulated edge and

δ_{max} is the maximum displacement of the edge for the chosen frequency ratio r.

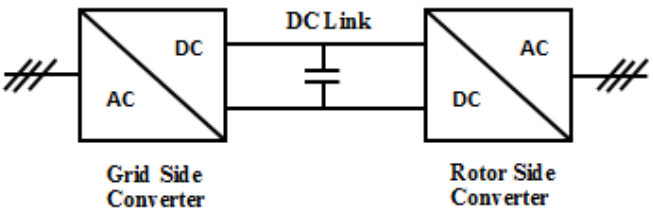

Figure 2.Two back-to-back PWM converters.

In the present scheme, the inverter output voltage is controlled, while its frequency is held constant at 50 Hz. In this range of operation, the PWM generator generates a carrier wave with frequency 15 times the fundamental frequency at the inverter output. Such a choice results in a line voltage waveform with 15 pulses per half cycle at the observed that the operating speed increases from inverter output. By modulating the carrier wave and hence the phase

voltages, the fundamental and harmonic voltage content can be varied. There are 15 pulses and 15 slots of 12° each. In each slot, two edges are modulated. For 100 % that modulation $(MI = 1)$, the maximum amount by which the edge can be modulated is $\delta_{max} = 6^{\circ}$. Any further displacement of the edge will cause the pulses in the modulated phase voltage to merge, resulting in a reduction of the number of pulses in the line voltage waveform (pulse dropping phenomenon).

7.0 Doubly Fed Induction Generator Wind Farm Model

Figure 3 shows the Simulink model of the single line diagram of the wind farm. Here, a 9-MW wind farm consisting of six 1.5 MW wind turbine connected to a 11kV distribution system exports power to a 33kV grid through a 30kM, 11kV feeder. A 2.3kV, 2 MVA plant consisting of a motor load (1.68MW induction motor at 0.93PF) and of a 200kW resistive load is connected on the same feeder at bus B11. The DC link voltage of the DFIG is also monitored.

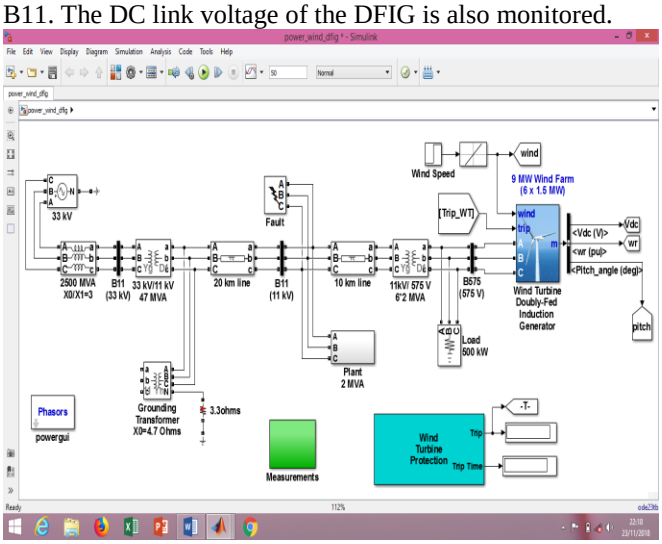

Figure 3. Simulink model of the DFIG wind farm.

Wind turbines use a doubly-fed induction generator (DFIG) consisting of a wound rotor induction generator and an AC/DC/AC IGBT-based PWM converter. The stator winding is connected directly to the 50Hz grid while the rotor is fed at variable frequency through the AC/DC/AC converter. The DFIG technology allows extracting maximum energy from the wind for low wind speeds by optimizing the turbine speed, while minimizing mechanical stresses on the turbine during gusts of wind. The optimum turbine speed producing maximum mechanical energy for a given wind speed is proportional to the wind speed. For wind speeds lower than 10m/s the rotor is running at sub-synchronous speed. At high wind speed it is running at hyper-synchronous speed.

The wind turbine is a phasor model that allows transient stability type studies with long simulation times. In this case, the system is observed during 50s. From the wind turbine block menu, four sets of parameters specified for the turbine, the generator and the converters (grid-side and rotor-side) are considered. The 6-wind-turbine farm is simulated by a single wind turbine block by multiplying the following three parameters by six, as follows:

1. The nominal wind turbine mechanical output: $6 * 1.5e6$ watts, specified in the Turbine data menu.
2. The generator rated power: $6 * 1.5/0.9$ MVA $(6 * 1.5\ MW\ at\ 0.9\ PF)$, specified in the Generator data menu.
3. The nominal DC bus capacitor: $6 * 10000$ microfarads, specified in the Converter data menu.

8.0 Simulation of a Fault on the 11kV System

In other to observe the impact of a single phase-to-ground fault occurring on the 11-kV line a B25 bus, a single phase-to- ground fault was initiated on phase A at time t = 5s using the "Fault" block. The fault is programmed to apply a 9-cycle single-phase to ground fault at time t = 5 s.

Setting the wind turbine at "Voltage regulation" mode, it was observed vividly from Figure 4 that the positive-sequence voltage at wind-turbine terminals (V1_B575) dropped to 0.8 pu during the fault, which is above the undervoltage protection threshold (0.75 pu for a t > 0.1 s). The wind farm therefore stays in service.

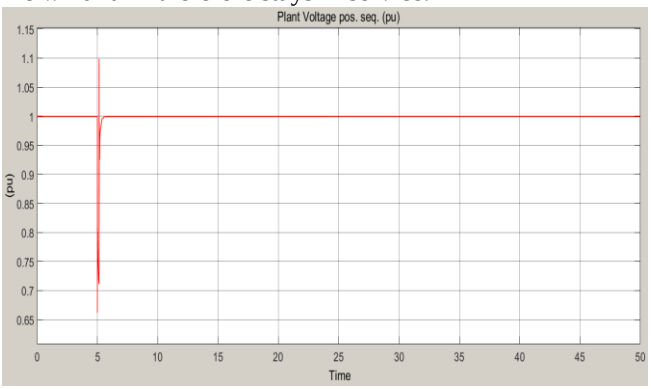

Figure 4.The positive-sequence voltage at wind-turbine terminals with the wind turbine at "Voltage regulation" mode

But when the wind turbine was set at "Var regulation" mode with Qref = 0, the voltage dropped below 0.7 pu and the undervoltage protection tripped off the wind farm.

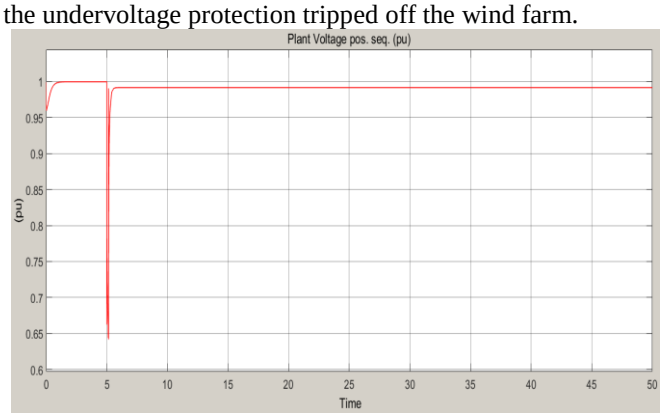

Figure 5. The positive-sequence voltage at wind-turbine terminals with the wind turbine at "Var regulation" mode

It can also be observed clearly from Figure 5 that the turbine speed increases. At time t = 40 s the pitch angle starts to increase in order to limit the speed as shown in Figure 6.

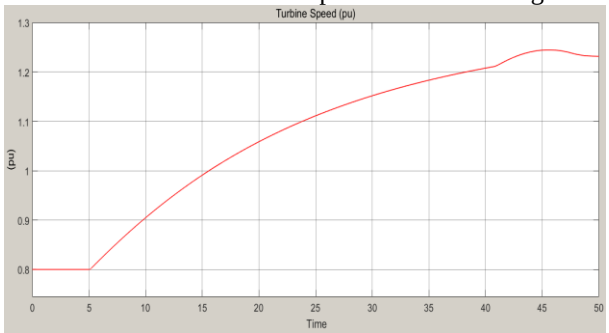

Figure 6. The wind-turbine speed with the wind turbine at "Var regulation" mode

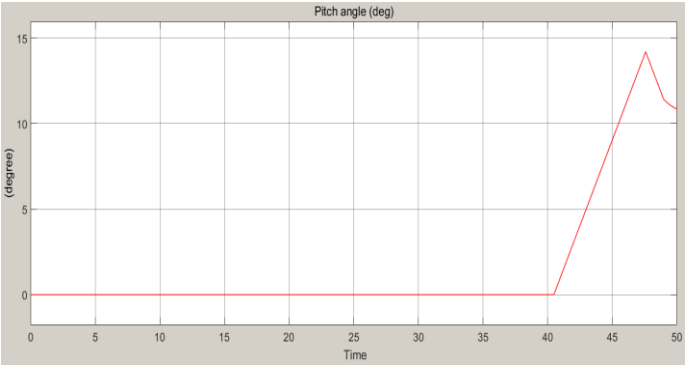

Figure 7.The wind-turbine pitch angle with the wind turbine at "Var regulation" mode.

9.0 Conclusion

Voltage stability analysis of grid connected wind farm system during occurrence of fault has been presented. DFIG were generally used in Wind farms because of their ability to supply power at constant voltage and frequency. Characteristics of DFIG were studied in MATLAB environment. Control techniques of DFIG have been studied also Magnitude and Frequency control has been studied and a Simulink model for the same has been proposed. Unlike traditional methods like Stator flux orientation vector control and magnitude and frequency control method manipulates the magnitude and frequency of the rotor voltage. This simplifies the design of the control system and improves system stability.

This work has been able to demonstrate the response of the system during occurrence of a short circuit fault on the line using AC/DC/AC IGBT-based PWM converter in DFIG has been obtained. The grid system voltage stability regulation was actually achieved as was seen by observing the response of the turbine to change in wind speed and through simulating the model for a voltage sag on the 132kV system and for a fault on the 11kV system.

References

Abdoune F., Aouzellag D., Ghedamsi K. (2016). Terminal voltage build-up and control of a DFIG based stand-alone wind energy conversion system. *Renew. Energy*, *97*, 468–480.

Ataji A.B., Miura Y., Ise T., Tanaka H. (2016). Direct Voltage Control with Slip Angle Estimation to Extend the Range of Supported Asymmetric Loads for Stand-Alone DFIG. *IEEE Trans. Power Electron.*, *31*, 1015–1025.

Erlich I., Feltes C., Shewarega F.Y. (2014). Enhanced voltage drop control by VSC-HVDC systems for improving wind farm fault Ridethrough capability. *IEEE Trans. Power Deliv.*, *29*, 378–385.

Hossain M. J., Pota H. R., Mahmud M. A. and Rodrigo A. Ramos. (2016). Investigation of the Impacts of Large-Scale Wind Power Penetration on the Angle and Voltage Stability of Power Systems

Kevin Z. H., Shady H.E., Ahmed F. Z. (2016). Voltage Stability Analysis of Grid-Connected Wind Farms with FACTS: Static and Dynamic Analysis

Mohsen G. Y. K. (2018). Improving voltage stability of wind farms connected to weak grids using facts. *A thesis submitted to the Faculty of Engineering at Cairo University in partial fulfillment of the requirements for the degree of master of science in electrical power and machines engineering*

Nguyen Tung Linh and Trinh Trong Chuong. (2015). Voltage Stability Analysis of Grids Connected Wind Generators. Conference Paper; DOI: 10.1109/ICIEA.2009.5138689 https://www.researchgate.net/publication/224546107

Rajiv Singh, Asheesh Kumar Singh, and Ashutosh Kumar Singh. (2012). Transient Stability Improvement of a FSIG Based Grid Connected Wind Farm with the help of a SVC and a STATCOM: A Comparison. *International Journal of Computer and Electrical Engineering, Vol.4, No.1.*

Ruchi Aggarwal, Sanjeev Kumar. (2014). Voltage Stability Improvement of Grid Connected Wind Driven Induction Generator Using SVC. *Int. Journal of Engineering Research and Applications* www.ijera.com *ISSN: 2248-9622, Vol. 4, Issue 5 (Version 2), pp.102-105*

Rui Melício1, Mendes V.M.F. (2017). Doubly Fed Induction Generator Systems for Variable Speed Wind Turbine. https://www.researchgate.net/publication/285295195

Shukla R. D., Tripathi R. K. (2014). A novel voltage and frequency controller for standalone DFIG based Wind Energy Conversion System. *Renew. Sustain. Energy Rev.*, *37*, 69–89.

Touaiti B., Azza H. B., Jemli M. (2015). Direct voltage control of stand-alone DFIG in wind energy applications. In Proceedings of the IEEE 16th International Conference on Sciences and Techniques of Automatic Control and Computer Engineering (STA), Monastir, Tunisia, 21–23 December; pp. 672–677.